

# Impact of Quarantine and Vaccination Policies on Viral Load

Dimitrios Koumatzidis <sup>1</sup>, Ioannis Seimenis <sup>2</sup>, Constantinos Loukas <sup>2,\*</sup> , Theodoros Constantinidis <sup>2</sup> and Adam Adamopoulos <sup>1</sup> 

<sup>1</sup> Medical Physics Laboratory, Department of Medicine, Democritus University of Thrace, 68133 Alexandroupolis, Greece

<sup>2</sup> Medical School, National and Kapodistrian University of Athens, 11527 Athens, Greece

\* Correspondence: cloukas@med.uoa.gr

**Abstract:** Epidemics and pandemics are a field of scientific research since ancient times. The intensity of the repeated phenomena demonstrates their cyclicity in time. The ongoing COVID-19 pandemic, also known as the coronavirus pandemic, confirmed observations made in previous disease outbreaks. Epidemics are mainly characterized by two factors: (a) the population dynamics and (b) the nature of the disease. This article uses continuous mathematical models, on the basis of a scalable compartmental approach, characterized by systems of ordinary differential equations under the condition that individuals can freely move from one compartment to another. Numerous experiments were carried out to examine the impact of quarantine and vaccination policies, separately or in combination, on cumulative viral load, a measure adopted to reflect the cumulative viral burden of an infected population for a given time period. Current findings demonstrate that quarantine may play a crucial role in controlling an epidemic at its early stages, as well as the importance of early and widespread implementation of a vaccination program. The suggested approach may be utilized to study specific quarantine and vaccination scenarios, by manipulating various parameters such as the duration and extent of social distancing measures or the effectiveness and compliance to vaccination policies, and thus assist in decision making.



**Citation:** Koumatzidis, D.; Seimenis, I.; Loukas, C.; Constantinidis, T.; Adamopoulos, A. Impact of Quarantine and Vaccination Policies on Viral Load. *Appl. Sci.* **2023**, *13*, 396. <https://doi.org/10.3390/app13010396>

Academic Editors: Andrea Ballini, Michele Covelli, Dario Di Stasio, Antonio Boccaccio and Maria Contaldo

Received: 22 November 2022

Revised: 16 December 2022

Accepted: 19 December 2022

Published: 28 December 2022



**Copyright:** © 2022 by the authors. Licensee MDPI, Basel, Switzerland. This article is an open access article distributed under the terms and conditions of the Creative Commons Attribution (CC BY) license (<https://creativecommons.org/licenses/by/4.0/>).

**Keywords:** viral load; epidemics; epidemic policy

## 1. Introduction

Pandemics, characterized by exponential disease growth affecting a wide geographical area, constitute a topic of interest since the Hippocrates era. Scientists are trying to confront pandemics mainly by developing treatments to cure the disease and by implementing measures of social distancing, such as quarantine, to restrict the spread of the virus [1]. Panois, a medieval pandemic that killed millions, had the characteristics of waves that demonstrated the cyclicity of infectious diseases [2]. The role of isolating infected individuals in the fight against Panois was crucial, saving thousands from death. Hansen's disease (also known as leprosy) which killed millions too, was satisfactorily tackled following the discovery of a suitable vaccine and subsequent mass vaccination. Nowadays, the relevant infectious bacteria have diminished but not erased. Leprosy is consistently present but limited to a particular region and with low numbers of infected individuals. Thus, it is now considered to be endemic [3,4].

In 1927, Kermack and McKendrick [5] published pioneer research about an epidemic, considered to be an unexpected increase in the number of disease cases in a specific geographical area. In the deterministic approach of the so-called SIR model, the entire population  $N$  is assumed constant and it is divided into three compartmental groups: Susceptible (S), Infected (I) and Recovered or Removed (R). Individuals are free to contact each other, and they are infected through contact with a rate of  $\alpha$ . There is no time delay in the exposure to the infecting agent (e.g., virus). Following recovery (or removal) of the infected individual, the subject is moved into the R group at a rate of  $\beta$ . The initial SIR

model was shaped to its current compartmental forms in 1978 [6]. Compartmental models, introduced to study epidemics, are either stochastic or deterministic. Stochastic models include elements of random variation and probability distributions, while deterministic ones give the same result every time they run since they consider average rates with no random deviations [7]. During the 1980s, studies based on network theory were also added to the epidemiology research arena [8]. Stochastic compartmental models and theoretical networks (random, small world, etc.) were combined to facilitate the study of epidemics in disease outbreaks, such as that of HIV. Both stochastic and deterministic models can employ either continuous or discrete formulations. The booming of computational power and software development in the last decades allowed scientists to represent models by systems of Ordinary Dynamical Equations (ODE) which can be solved numerically [9].

Contemporary policies to eliminate a pandemic can be grouped into two main categories. Quarantine and vaccination policies [10]. Quarantine policies can implement either as prevention or contagion rehabilitation of an infection. It is the movement restriction of persons who are presumed to have been exposed to a contagious disease but are not ill, either because they did not become infected or because they are still in the incubation period. Isolation, containment and social distancing are also some other public health policies to control epidemics [11]. Vaccination policies are the decision to vaccinate individuals and provide immunity to the communities. Decision-makers should take into account factors such as time of vaccination, age groups and vaccine ethics [12]. In this study the vaccines are similar and vaccination effects are the same for all.

Viral load is the amount of strain in the body of an individual. Its value is connected to the severity of the disease and the shedding volume [13]. Current studies in the viral load focus on comparing various individual viral loads and their role in the epidemic's evolution [14,15], as in the COVID-19 epidemic [16]. Researchers try to study the kinetics of the using mostly stochastic models [17]. However, it is also important to take into account the total viral load in the community and its dependence on quarantine and vaccination policies that may be applied.

In the current work, a scalable compartmental approach based on ODE systems is applied to study viral and/or bacterial load in a pandemic, under the condition that individuals can freely move from one compartment to another. Initially, we examine the viral load in the original SIR system. Secondly, we introduce a model with a cyclic (waving) approach. Then, we add the quarantine and vaccination procedures, separately or in combination, to study the beneficial impact of respective policies. The equilibrium states are investigated, as well as their dependence on the different policies. The viral load in each model is determined and is used as a marker for inter-model comparisons and for monitoring the pandemic evolution.

## 2. Materials and Methods

### 2.1. The SIR Model

The epidemic process in the SIR model is schematically represented in Figure 1. As shown, a fraction of the subpopulation  $S$  turns to  $I$  with rate  $\alpha$  and another fraction of the subpopulation  $I$  turns to  $R$  with rate  $\beta$ .

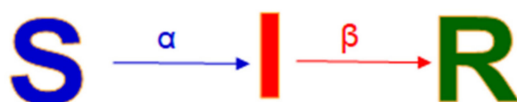


**Figure 1.** Schematic representation of the SIR model.

The total size of the population  $N$  is given by:

$$N = S + I + R \quad (1)$$

Moreover,  $N$  is normalized. So, we set  $N = 1$ ; therefore, the  $S$ ,  $I$  and  $R$  stand as a fraction of the population.

We denote:

$$\frac{dS}{dt} = \text{rate of Susceptible over time} \tag{2}$$

$$\frac{dI}{dt} = \text{rate of Infected over time} \tag{3}$$

$$\frac{dR}{dt} = \text{rate of Recovered (removed) over time} \tag{4}$$

According to Figure 1 and Equations (2)–(4), the system of ODEs describing the SIR model is:

$$\begin{aligned} \frac{dS}{dt} &= -aSI \\ \frac{dI}{dt} &= aSI - \beta I \\ \frac{dR}{dt} &= \beta I \end{aligned} \tag{5}$$

We can easily prove from the ODE that  $\lim_{t \rightarrow \infty} S$ ,  $\lim_{t \rightarrow \infty} I$ ,  $\lim_{t \rightarrow \infty} R$  exist. From Equation (5) we obtain

$$\begin{aligned} \frac{dS}{dt} &= -aS \frac{dR}{\beta} \\ \frac{dS}{dR} &= -\frac{aS}{\beta} \\ \frac{dS}{S} &= -\frac{a}{\beta} dR \\ \ln S &= -\frac{a}{\beta} R + c \\ S &= S_0 \exp\left(-\frac{a}{\beta} R\right) \end{aligned} \tag{6}$$

Since  $0 < R < 1$ , susceptible individuals are

$$\lim_{t \rightarrow \infty} S = \lim_{t \rightarrow \infty} S_0 \exp\left(-\frac{a}{\beta} R\right) \rightarrow S_{t \rightarrow \infty} > 0 \tag{7}$$

Equation (5) results in:

$$\begin{aligned} \frac{dS}{dI} &= -\frac{aS}{aS-\beta} \\ \frac{dI}{dS} &= -\frac{aS-\beta}{aS} \\ dI &= -dS + \frac{\beta dS}{aS} \\ \int dI &= \int -dS + \int \frac{\beta dS}{aS} \\ I &= -S + \frac{\beta}{\alpha} \ln S + c \end{aligned} \tag{8}$$

Equation (8) indicates that I at infinity will be 0 since it is assumed that all individuals will again fall within the S group.

The SIR model has an equilibrium solution at

$$\lim_{t \rightarrow \infty} (S(t), I(t), R(t)) \tag{9}$$

The solution of the above system for S, I, and R is at time  $S(\infty)$

$$S(\infty) = S(0) \times \exp\left(-\frac{a}{\beta}(1 - S_\infty)\right) \rightarrow 0 \tag{10}$$

$$R(\infty) = 1 - S(\infty) \rightarrow 1 \tag{11}$$

$$I(\infty) = 0 \tag{12}$$

where  $S_0$  and  $I_0$  are the initial conditions and regarding inter-compartmental rates,  $a > \beta$  is assumed. The above solution also shows that moving to infinity a number of Susceptible and a number of Recovered individuals will be present.

### 2.2. The CSIR Model

To facilitate decision-making under real conditions, the basic SIR model was gradually enhanced by adding extra inter-compartmental interactions and/or compartments. The CSIR model employed in this work is based on the widely known as the SIRS model [18,19].

Thus, as a second step, we considered the loss of immunity by amending the system accordingly. Individuals from the R group are re-transferred to the S group with a constant  $\gamma$ , while the SIR notation and assumptions are maintained.

The system named CSIR (Circular SIR) is shown in Figure 2.

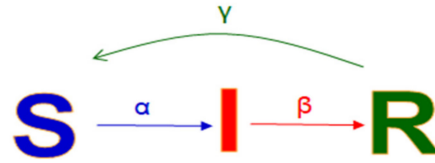


Figure 2. Schematic representation of the CSIR model.

Based on Equation (5) of the original SIR model, the ODE that describes the CSIR system is the following:

$$\begin{aligned} \frac{dS}{dt} &= -aSI + \gamma R \\ \frac{dI}{dt} &= aSI - \beta I \\ \frac{dR}{dt} &= \beta I - \gamma R \end{aligned} \tag{13}$$

The CSIR model has an infection-free equilibrium when  $\frac{dS}{dt} = 0, \frac{dI}{dt} = 0, \frac{dR}{dt} = 0$  and  $S = 1, I = 0, R = 0$ .

A steady-state solution of this ODE system also exists for  $I \neq 0$ . By denoting  $S^{ss}, I^{ss}$  and  $R^{ss}$  the steady state solution for the S, I and R subpopulations, respectively, the system is given by the following equations:

$$S^{ss} = \frac{\beta}{\alpha} \tag{14}$$

$$I^{ss} = \frac{1 - \frac{\beta}{\alpha}}{1 + \frac{\alpha}{\gamma}} \tag{15}$$

$$R^{ss} = \frac{\beta I}{\gamma} \tag{16}$$

Equations (14)–(16) give steady states as an expression of the coefficients  $\alpha, \beta, \gamma$  of the model.

### 2.3. The CSIRQ Model

When a disease is turning into an epidemic, one of the basic measures available to restrict it is the implementation of quarantine, which may also turn into a curfew. By incorporating the quarantine, the CSIR model transforms into the CSIRQ one. As shown in Figure 3, a new compartment of individuals that are quarantined (Q) is added, which is fed by the S group with a rate of  $\delta$ . A counter transfer, from Q to S, with rate  $\mu$  is also assumed. The rate  $\zeta$  corresponds to the repositioning of infected individuals from I to Q, whilst the rate  $\iota$  characterizes the transition from the Q group to the R compartment. The rate  $\zeta$  should equal the rate  $\alpha$ , but, in general, it is assumed that not all infected individuals comply with the social distancing and quarantine measures. Therefore, the CSIRQ model can be described by the following ODE system:

$$\begin{aligned} \frac{dS}{dt} &= -aSI + \gamma R - \delta S + \mu Q \\ \frac{dI}{dt} &= aSI - \beta I - \zeta I \\ \frac{dR}{dt} &= \beta I - \gamma R + \iota Q \\ \frac{dQ}{dt} &= \delta S + \zeta I - \mu Q - \iota Q \end{aligned} \tag{17}$$

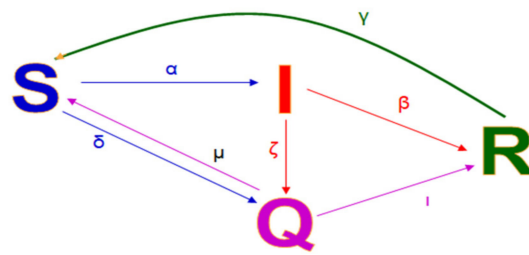


Figure 3. Schematic representation of the CSIRQ model.

2.4. The CSIRV Model

In the next step of the proposed methodology, an alternative compartment is introduced into the CSIR model, that of the vaccinated individuals. We denote the group of vaccinated individuals as V and the new model, schematically represented in Figure 4, as CSIRV.

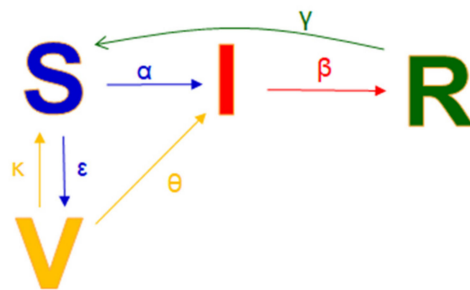


Figure 4. Schematic representation of the CSIRV model.

We assume that the vaccinated group has social contact with infected individuals and, therefore, we set  $\theta$  as the rate of vaccinated individuals that become infected.

It is also assumed that individuals in the S compartment are repositioned in V with a constant rate  $\epsilon$  that depends on the vaccination scheme adopted. We also assume that vaccinated individuals may relapse to compartment S due to various reasons (e.g., loss of immunity, ineffective vaccination) with a constant rate  $\kappa$ . The CSIRV model is described by the following ODE system:

$$\begin{aligned} \frac{dS}{dt} &= -aSI + \gamma R - \epsilon S + \kappa V \\ \frac{dI}{dt} &= aSI + \theta IV - \beta I \\ \frac{dR}{dt} &= \beta I - \gamma R \\ \frac{dV}{dt} &= \epsilon S - \theta IV - \kappa V \end{aligned} \tag{18}$$

Considering that initially, the recovered individuals are zero and that the number of infected is small, we can set:

$$S = 1 - V \tag{19}$$

which indicates that each subject is either vaccinated or not at initial conditions.

Before the viral outbreak, the steady is free of infected individuals,  $R_0 = 0$

$$\begin{aligned} S^{SS} &= -aSI + \gamma R - \epsilon S + \kappa V \\ I^{SS} &= aSI + \theta IV - \beta I \\ R^{SS} &= \beta I - \gamma R \\ V^{SS} &= \epsilon S - \theta IV - \kappa V \end{aligned} \tag{20}$$

One free of the infected steady state exists, i.e.,

$$1 = S + I + R + V \tag{21}$$

and assuming that a part of the population is vaccinated, the subpopulations at a steady state will be

$$Initial\ SS = [S, 0, 0, 1 - V] \tag{22}$$

There is another steady state for  $I \neq 0$ , under the assumption ( $\beta > \alpha$ ), which will be reached after a sufficient time interval and will turn the pandemic into an endemic.

Assuming that all susceptible individuals were vaccinated, the steady state for  $I \neq 0$  is described by

$$\begin{aligned} \frac{dI}{dt} &= aSI + \theta IV - \beta I \\ 0 &= I(\alpha S + \theta V - \beta) \\ S^{ss} &= \frac{\beta - \theta V^{ss}}{\alpha}, \quad (S^{ss} = V^{ss}) \\ S^{ss} &= \frac{\beta}{\alpha + \theta} \end{aligned} \tag{23}$$

### 2.5. The CSIRQV Model

The CSIRQV model combines all five compartments discussed above into a general, comprehensive model. Considering that inter-compartmental interactions are characterized by the constant rates  $\alpha, \beta, \gamma, \delta, \epsilon, \zeta, \eta, \theta, \iota, \kappa, \lambda$  and  $\mu$ , where  $\eta$  and  $\lambda$  relate to the interactions between the Q and V compartments. The CSIRQV model can be described by the following ODE system:

$$\begin{aligned} \frac{dS}{dt} &= -aSI + \gamma R - \epsilon S + \kappa V - \delta S + \mu Q \\ \frac{dI}{dt} &= aSI + \theta IV - \beta I - \zeta I \\ \frac{dR}{dt} &= \beta I - \gamma R + \iota Q \\ \frac{dV}{dt} &= \epsilon S - \theta IV - \kappa V - \eta V + \lambda Q \\ \frac{dQ}{dt} &= \delta S + \zeta I + \eta V - \lambda Q - \mu Q - \iota Q \end{aligned} \tag{24}$$

The above system is illustrated in Figure 5.

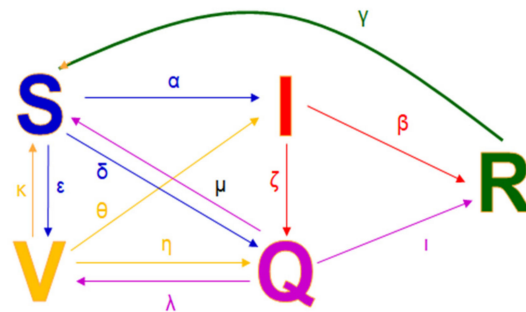


Figure 5. Schematic representation of the CSIRQV model.

The CSIRQV model has difficulty finding solutions. To examine the equilibrium of the system and then estimate its steady-state parameters, we first have to estimate the Jacobian matrix of the system, which is given by

$$J = \begin{bmatrix} \left(\frac{\partial S}{\partial t}\right) & \left(\frac{\partial S}{\partial I}\right) & \left(\frac{\partial S}{\partial R}\right) & \left(\frac{\partial S}{\partial V}\right) & \left(\frac{\partial S}{\partial Q}\right) \\ \left(\frac{\partial I}{\partial t}\right) & \left(\frac{\partial I}{\partial I}\right) & \left(\frac{\partial I}{\partial R}\right) & \left(\frac{\partial I}{\partial V}\right) & \left(\frac{\partial I}{\partial Q}\right) \\ \left(\frac{\partial R}{\partial t}\right) & \left(\frac{\partial R}{\partial I}\right) & \left(\frac{\partial R}{\partial R}\right) & \left(\frac{\partial R}{\partial V}\right) & \left(\frac{\partial R}{\partial Q}\right) \\ \left(\frac{\partial V}{\partial t}\right) & \left(\frac{\partial V}{\partial I}\right) & \left(\frac{\partial V}{\partial R}\right) & \left(\frac{\partial V}{\partial V}\right) & \left(\frac{\partial V}{\partial Q}\right) \\ \left(\frac{\partial Q}{\partial t}\right) & \left(\frac{\partial Q}{\partial I}\right) & \left(\frac{\partial Q}{\partial R}\right) & \left(\frac{\partial Q}{\partial V}\right) & \left(\frac{\partial Q}{\partial Q}\right) \end{bmatrix} \tag{25}$$

By applying Equation (25) to the system of Equation (24), we derive:

$$J = \begin{bmatrix} -aI - \varepsilon - \delta & -\alpha S & \gamma & \kappa & \mu \\ \alpha I & \alpha S + \theta V - \beta - \zeta & 0 & i\theta & 0 \\ 0 & \beta & \gamma & 0 & i \\ \varepsilon & \theta I & 0 & i\theta - \kappa - \eta & \eta \\ \delta & \zeta & 0 & \eta & -\lambda - \mu - 1 \end{bmatrix} \quad (26)$$

which can identify the stability of the steady states [20,21].

### 2.6. Estimation of Viral Load

To facilitate the comparison between the different models and scenarios studied, the relative measure of cumulative viral load, CVL(t), is adopted. CVL(t) reflects the cumulative viral burden of the infected population for a given period of time, t. If each infected individual carries a mean individual viral load, m, considered to be stable and identical for all individuals, then CVL(t) is provided by Equation (27).

$$CVL(t) = m \int_0^t I(t)dt \quad (27)$$

In a simplified approach  $m = 1$  and Equation (27) reduces to the total number of infected individuals over the time period, t.

## 3. Results

### 3.1. The SIR Model

Figure 6 presents typical results for the original SIR model figuring the S, I and R dynamics of an epidemic. In this case, as well as in the following ones, the rates  $\alpha$  and  $\beta$  have been assumed equal to 0.18 and 0.06, respectively, according to the statistical analysis made with data from COVID Live—Coronavirus Statistics—Worldometer worldometers.info) in order to match the COVID19 pandemic [22].

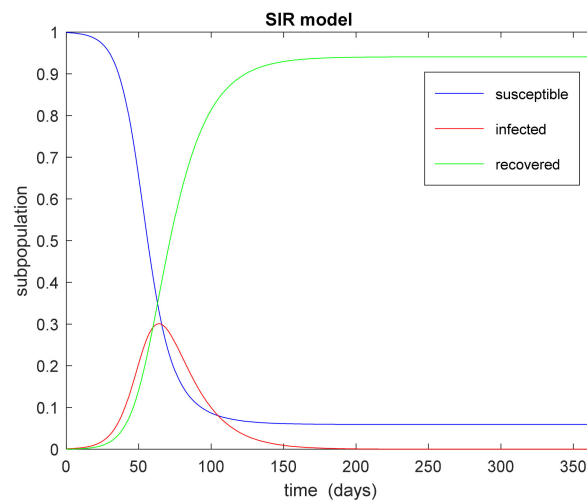


**Figure 6.** Typical dynamics of the SIR model for the following constant rates:  $\alpha = 0.18$ ,  $\beta = 0.06$ . Cumulative Viral load (t = 365): 15.67.

If  $\beta$  converges towards  $\alpha$  (e.g.,  $\alpha = 0.18$ ,  $\beta = 0.18$ ), then the viral load reduces to 0.24, suggesting that the system transforms to aninfected-free state.

### 3.2. The CSIR Model

In the CSIR model, if we assume that  $\beta$  and  $\gamma$  rates are constant and much lower than  $\alpha$ , then the relatively high  $\alpha$  rate drives towards lower S and higher I. Figure 7 demonstrates the cyclic waves of the model, for  $\alpha$  and  $\beta$  values that equal those used in Figure 6. It is

evident that the viral load increases by 88%, even for a relatively low rate of individual repositioning from R to S ( $\gamma = 0.006$ ).

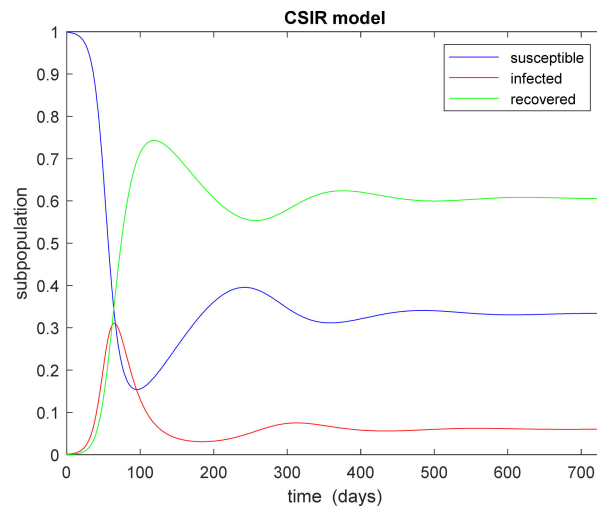


**Figure 7.** Typical dynamics of the CSIR for the following constant rates  $\alpha = 0.18$ ,  $\beta = 0.06$ ,  $\gamma = 0.006$  (see Figure 2 for notation of rates); Cumulative viral load = 29.48 (for  $t = 365$ ).

For a relatively high  $\beta = 0.12$  (double that adopted in Figure 7) and assuming unchanged  $\alpha$  and  $\gamma$  rates (i.e., equal to those applied in Figure 7), the I compartment diminishes and the viral load decreases by 76%. With regard to the  $\gamma$  rate and assuming that  $\alpha$  and  $\beta$  rates remain unchanged, a  $\gamma$  value of 0.012 (double that adopted in Figure 7) increases not only S but also I, according to Equation(11). As a result, viral load increases by 49%.

Since we set  $\beta < \alpha$ , there is an epidemic that finally turns to an endemic equilibrium where  $I^{ss} > 0$ . Figures 8 and 9 display the steady state phase portraits for S against I and I against R, respectively.

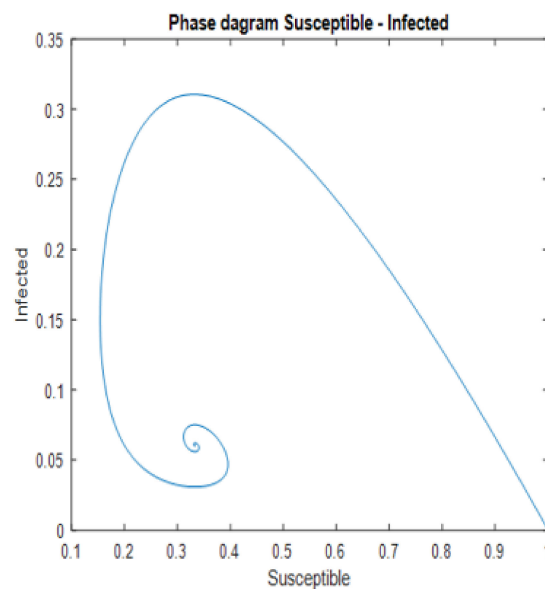


**Figure 8.** Phase portrait of I against S, for the stable state of the CSIR model.

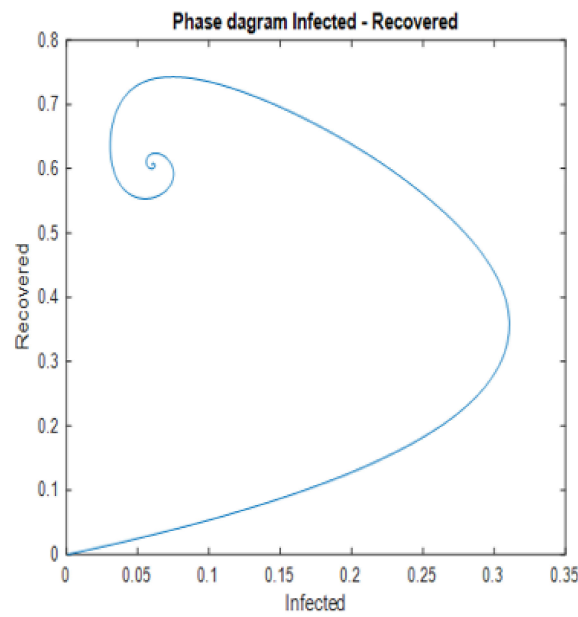


**Figure 9.** Phase portrait of R against I, for the stable state of the CSIR model.

### 3.3. The CSIRQ Model

Setting up a quarantine policy leads to the CSIRQ model. The time evolution of the S, I, R and Q compartments, keeping the  $\alpha$ ,  $\beta$  and  $\gamma$  rates unchanged and implementing quarantine to the infected individuals at a rate  $\zeta = 0.06$  (I to Q) and employing a Q to R rate of  $i = 0.06$ , is depicted in Figure 10. The employed  $\zeta$  rate of 0.06 assumes a time interval of 15 days covering both the incubation and infection periods.

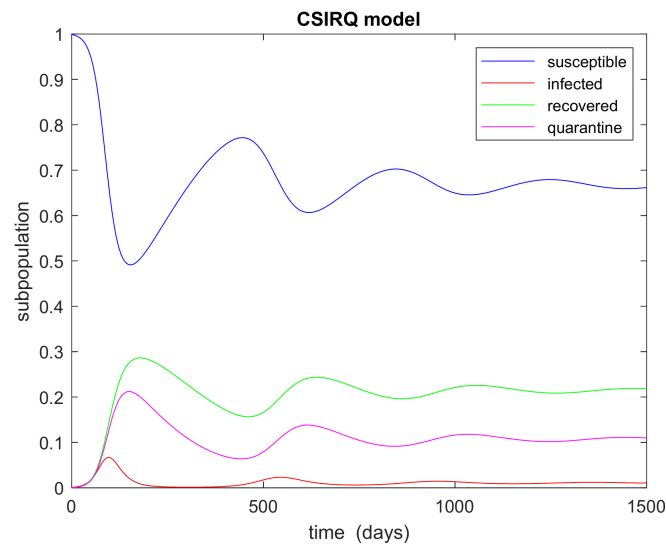


**Figure 10.** Typical dynamics of the CSIRQ for the following constant rates  $\alpha = 0.18$ ,  $\beta = 0.06$ ,  $\gamma = 0.006$ ,  $\zeta = 0.06$ ,  $\iota = 0.006$ ,  $\mu = 0$ ,  $\delta = 0$ , Cumulative viral load = 5.68 (for  $t = 365$  days).

Figure 10 shows the dynamics of compartments over a time interval of 1500 days. There are four peaks, one every year, where they drive to increase the quarantine of individuals. Steady-state is achieved at about  $t = 1500$  days when the number of infected individuals stabilizes, and the disease is regarded as endemic.

By implementing quarantine not only for the infected individuals but also for the susceptible ones, the infected population decreases sharply. This is demonstrated in Figure 11, which depicts the time evolution of the S, I, R and Q compartments, after

introducing the rates  $\delta = 0.001$  and  $\mu = 0.0001$  that describe the interaction between Q and S compartments (Figure 3).

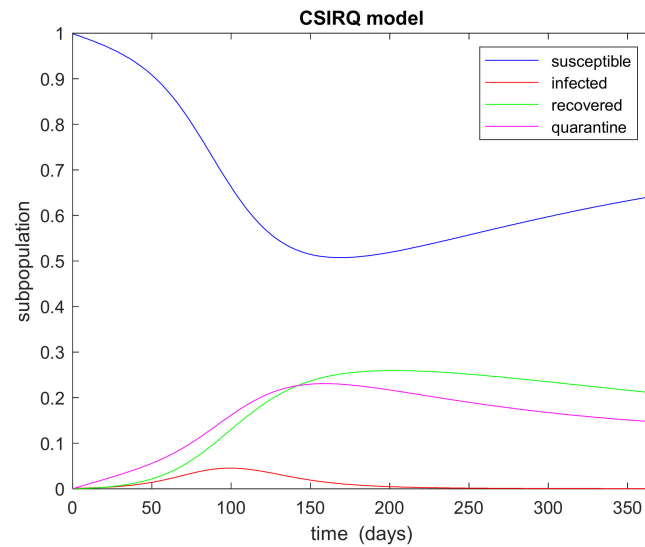


**Figure 11.** Typical dynamics of the CSIRQ model for the following constant rates ( $\alpha = 0.18$ ,  $\beta = 0.06$ ,  $\gamma = 0.006$ ,  $\delta = 0.001$ ,  $\mu = 0.0001$ ,  $\zeta = 0.06$ ,  $\iota = 0.006$ , Cumulative viral load = 4.32 (for  $t = 365$  days)).

Figure 11 illustrates the dynamics of the compartments in the CSIRQ model. Estimated waves are weaker compared to the corresponding ones presented in Figure 10. The first peak of I, at  $t = 99$  days,  $I = 0.048$ , is lower than the first peak of Figure 10 at  $t = 99$   $I = 0.067$ , thus resulting in lower R from  $R = 0.22$  shown in Figure 10 to  $R = 0.18$  displayed in Figure 11.

Figure 12 presents the steady state phase portrait for S against I. The rates are identical to those corresponding to Figure 11, with  $t$  being equal to 1500 days.

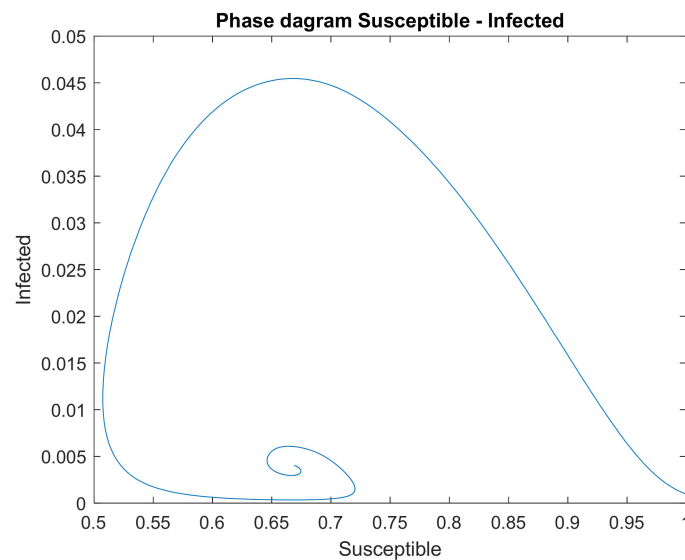


**Figure 12.** Phase portrait of I against S for the CSIRQ model.

### 3.4. The CSIRV Model

The dynamics of the CSIRV model, incorporating compartment V, is shown in Figure 13.

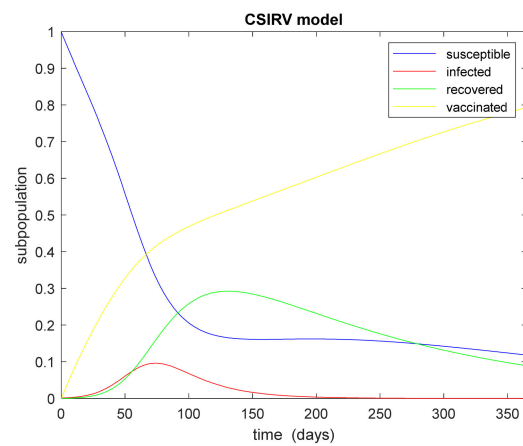


**Figure 13.** Dynamics of the CSIRV model ( $\alpha = 0.18, \beta = 0.06, \gamma = 0.006, \varepsilon = 0.008333, \theta = 0.0006, \kappa = 0.00008333$ ). Cumulative Viral load = 7.56 (for  $t = 365$  days).

Figure 13 depicts the time evolution of the S, I, R and V compartments, after introducing the rates  $\varepsilon = 0.008333, \kappa = 0.00008333$  and  $\theta = 0.0006$  that describe the interaction among V, S and I compartments (Figure 4). The adopted value of rate  $\varepsilon$  assumes that all individuals in the population get vaccinated within 4 months from the outbreak onset. According to the model, the rate of vaccinated people is stable. That means that the number of vaccinated individuals every day is lower. The adopted rate  $\kappa$  assumes a 1/1000 vaccine failure, whilst the rate  $\theta = 0.0006$  assumes a moderate loss of immunity. The viral load was found to be 7.56 365 days post-onset.

### 3.5. The CSIRVQ Model

The comprehensive CSIRVQ model combines both quarantine and vaccination policies and, thus, the V and Q compartments are included, as shown in Figure 5. Using the main rates mentioned above, the model’s dynamics are depicted in Figure 14. As seen, the number of infected individuals reaches the first peak at approximately date 40 which, however, is extremely low resulting in a viral load of 0.23.

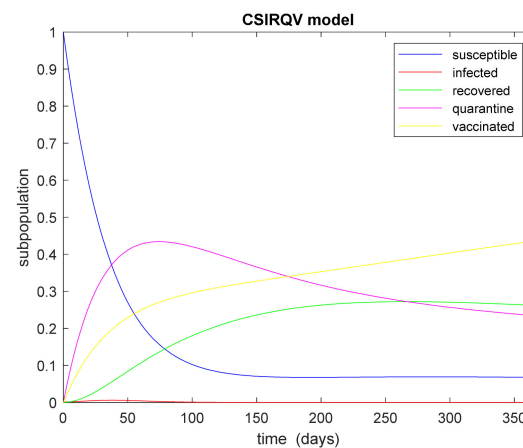


**Figure 14.** Dynamics of the CSIRVQ model ( $\alpha = 0.18, \beta = 0.06, \gamma = 0.006, \delta = 0.001, \varepsilon = 0.008333, \zeta = 0.06, \eta = 0.0001, \theta = 0.0006, \iota = 0.006, \kappa = 0.00008333, \lambda = 0.00001, \mu = 0.0001$ ). Cumulative Viral load: 0.23 ( $t = 365$  days).

### 3.6. Viral Load

Table 1 presents estimations of the cumulative viral load in different experiments of the CSIRQ model keeping the rates of the CSIR model ( $\alpha, \beta, \gamma$ ) constant.

**Table 1.** Cumulative Viral load estimations for different scenarios of the CSIRQ model (t = 365 days).

Model	Rates	Cumulative Viral Load
CSIRQ	$\alpha = 0.18, \beta = 0.06, \gamma = 0.006,$ $\delta = 0.001, \mu = 0.0001, \zeta = 0.06,$ $\iota = 0.006$	4.32
CSIRQ_1	$\alpha = 0.18, \beta = 0.06, \gamma = 0.006,$ $\delta = 0.002, \mu = 0.0002, \zeta = 0.06,$ $\iota = 0.006$	3.02
CSIRQ_2	$\alpha = 0.18, \beta = 0.06, \gamma = 0.006,$ $\delta = 0.0005, \mu = 0.00005, \zeta = 0.06,$ $\iota = 0.006$	4.99

CSIRQ viral load of the basic scenario presented in Figure 11 results in a viral load of 4.32. In the CSIRQ\_1 scenario, the  $\delta$  and  $\mu$  rates are doubled (0.002 and 0.0002, respectively) compared to the basic situation. An increase in  $\delta$  represents a tighter quarantine policy, although  $\mu$  (from Q to S) is also assumed to increase in a realistic approach. In the CSIRQ\_2 scenario, the  $\delta$  and  $\mu$  rates are sub doubled (0.0005 and 0.00005, respectively) compared to the basic situation, thus representing a more relaxed quarantine policy. As seen viral load decreases by 26% in CSIRQ\_1 and increases by 16% in CSIRQ\_2 in relation to the reference CSIRQ, although viral loads remain relatively low in all situations.

Similarly, Table 2 presents estimations of the viral load in different experiments of the CSIRV model keeping the rates of the CSIR model ( $\alpha, \beta, \gamma$ ) constant. Apart from the basic vaccination scenario, graphically depicted in Figure 13, two additional vaccination strategies are examined. In all three situations, vaccination starts at time zero. In the CSIRV\_1 scenario representing a higher vaccination compliance in relation to the standard scenario, rates  $\epsilon$  (S to V) and  $\kappa$  (V to S) are doubled (0.016666 and 0.00016666, respectively) compared to the corresponding values in the basic CSIRV model. As a result, the viral load reduces by a factor of 3. On the other hand, subdoubling the  $\epsilon$  and  $\kappa$  rates in the CSIRV\_2 scenario (0.004167 and 0.00004167, respectively) almost doubles the viral load in relation to the reference scenario.

**Table 2.** Cumulative Viral load estimations for different scenarios of the CSIRV model (t = 365 days).

Model	Rates	Cumulative Viral Load
CSIRV	$\alpha = 0.18, \beta = 0.06, \gamma = 0.006$ $\epsilon = 0.008333, \theta = 0.0006,$ $\kappa = 0.00008333$	7.56
CSIRV_1	$\alpha = 0.18, \beta = 0.06, \gamma = 0.006$ $\epsilon = 0.016666, \theta = 0.0006,$ $\kappa = 0.00016666$	1.64
CSIRV_2	$\alpha = 0.18, \beta = 0.06, \gamma = 0.006$ $\epsilon = 0.004167, \theta = 0.0006,$ $\kappa = 0.00004167$	14.01

#### 4. Discussion

Combining CSIRQ and CSIRV leads to the CSIRVQ model (Figure 5). Many runs were conducted to check stability from phase portraits. It was found that all equilibriums were unstable as shown in Figure 12.

A comparison of the results obtained from the basic CSIR, CSIRQ and CSIRV models presented in Figures 7, 11 and 13, respectively, indicate that either quarantine or vaccination effectively reduces viral load in relation to the basic CSIR scheme (29.48), with quarantine being more powerful than vaccination under the specific conditions studied (4.32 vs. 7.56). Undoubtedly, combining both quarantine and vaccination policies drastically reduces viral load to 0.23 (Figure 14) under the same conditions. Table 3 also presents two alternative scenarios for the CSIRQV model. In the CSIRQV\_1 scenario, the rates  $\delta$  (S to Q) and  $\mu$  (Q to S) are increased by an order of magnitude to describe a more severe quarantine protocol

than the basic one. The resultant viral load is 0.09, demonstrating the pivotal role that social distancing can play in diminishing the infected subpopulation. In the CSIRQV\_2 scenario, there is no interaction between the S and Q compartments ( $\delta = 0$  and  $\mu = 0$ ). In this case, the viral load obtains a value of 0.27, close to the corresponding value of the basic scenario. It is assumed, therefore, that social distancing measures on the susceptible individuals have a minor impact on the overall viral load in a comprehensive scenario also incorporating vaccination.

**Table 3.** Viral Load estimations for different scenarios of the CSIRQV model (t = 365 days).

Model	Model Parameters of the Model	Cumulative Viral Load
CSIRQV	$\alpha = 0.18, \beta = 0.06, \gamma = 0.006$ $\delta = 0.001, \epsilon = 0.008333, \zeta = 0.06,$ $\eta = 0.0001, \theta = 0.0006, \iota = 0.006,$ $\kappa = 0.00008333, \lambda = 0.00001,$ $\mu = 0.0001$	0.23
CSIRQV_1	$\alpha = 0.18, \beta = 0.06, \gamma = 0.006$ $\delta = 0.01, \epsilon = 0.008333, \zeta = 0.06,$ $\eta = 0.0001, \theta = 0.0006, \iota = 0.006,$ $\kappa = 0.00008333, \lambda = 0.00001,$ $\mu = 0.001$	0.09
CSIRQV_2	$\alpha = 0.18, \beta = 0.06, \gamma = 0.006, \delta = 0,$ $\epsilon = 0.008333, \zeta = 0.06, \eta = 0.0001,$ $\theta = 0.0006, \iota = 0.006,$ $\kappa = 0.00008333, \lambda = 0.00001, \mu = 0$	0.27

This research attempts to provide a generalized approach that may be of interest in studying epidemics and in providing insights with regard to the effect that various policies, such as vaccination and quarantine, may have on the cumulative viral load. The proposed approach allows for the consideration of combined policies and different levels of vaccination compliance and quarantine stringency. It also allows for studying the crucial role of time parameters, such as the timepoint of adoption of constraining measures, or other factors, such as vaccination coverage and the emergence of vaccine resistance, that may play in epidemic control. By incorporating realistic statistical data and/or data from molecular biology into the model, the proposed approach may provide a useful decision-making tool for mitigating or suppressing a viral epidemic or pandemic.

Current results (Table 1) reveal that quarantine plays an important role in the first stages of an epidemic. Our findings are in good agreement with those of other studies which have shown that stringent restrictions in the quarantine framework reduce the infected subpopulation [23,24]. With regard to vaccination, the current study assumed that all vaccines available possess the same effectiveness and that they build immunity to the same extent in all individuals. It demonstrated, however, the pivotal role of a successful vaccination program in eliminating an epidemic wave (Table 3). Other studies have also shown that efficient vaccination programs with high compliance rates lead to disease restriction. [25]. Moreover, a recently published study [26,27] based on a stochastic approach has confirmed that social distancing measures can be relaxed after the successful implementation of a vaccination program [28].

The above analysis suggests that the proposed straightforward approach can be easily implemented to examine in-silico different pandemic or epidemic situations and infer conclusions that may facilitate decision-making. Nevertheless, realistic rates based on real-world data have to be employed to carry out reliable simulations. Viral load seems to be a feature that can provide insights into the disease evolution and can largely facilitate inter-comparisons between models and/or between different scenarios within the same model. Viral load estimation for a certain period of time constitutes a useful tool for physicians and policymakers to decide on precautionary measures and for physicians to plan and develop therapeutic interventions. Policymakers can weigh the potential benefits of certain policies against the costs emanating from the employment of such policies.

This work suffers from certain limitations [29,30]. In the CSIRQV model studied several assumptions have been made (e.g., constant inter-compartmental rates were assumed, although involved rates, such as the infection to recovery rate,  $\beta$ , may be time-dependent; seasonal infection was not considered; no time-delays in vaccination were examined; immunity waning was not investigated; variable social contact was not considered). Additionally, validation of the described models with real-world data was not performed, in particular, with regard to rates  $\eta$ ,  $\lambda$  and  $\iota$ . However, the main scope of the current study was to computationally approach the relevant models available and highlight their differences rather than validating specific models with data that may be subject to under-reporting. A vaccine-resistant mutation virus was not studied separately from a wild-type virus and, subsequently, different mutation rates were not considered.

## 5. Conclusions

The proposed approach seems to be able to study different scenarios regarding the onset and the evolution of an epidemic or a pandemic before resulting in an endemic. This approach could also be utilized to investigate the mutation of the initial virus into various strains if we consider the mutation strain as a new disease. The normalized viral load adopted in this study seems to be a simple and efficient marker for disease monitoring, which allows for intercomparison between different models and, thus, facilitates benchmarking of different policies and strategies.

**Author Contributions:** Conceptualization, D.K., I.S. and A.A.; Methodology, D.K., I.S., C.L., T.C. and A.A.; Software, D.K., T.C. and A.A.; Validation, D.K., I.S., C.L., T.C. and A.A.; Formal Analysis, D.K., I.S., C.L., T.C. and A.A.; Investigation, D.K., I.S., C.L., T.C. and A.A.; Resources, D.K., I.S. and A.A.; Data Curation, D.K.; Writing—Original Draft Preparation, D.K., I.S., C.L., T.C. and A.A.; Writing—Review and Editing, D.K., I.S., C.L., T.C. and A.A.; Visualization, D.K., T.C. and A.A.; Supervision, I.S. and A.A.; Project Administration, I.S. and A.A.; Funding Acquisition, A.A. All authors have read and agreed to the published version of the manuscript.

**Funding:** This research received no external funding.

**Institutional Review Board Statement:** Not applicable.

**Informed Consent Statement:** Not applicable.

**Data Availability Statement:** Data available within the article.

**Conflicts of Interest:** The authors declare no conflict of interest.

## References

1. Tsiamis, K. Historical and Epidemiological Approach of Plague during Byzantine Times (330–1453 a. D.). Ph.D. Thesis, National and Kapodistrian University of Athens, Athens, Greece, 2010; pp. 87–132. [CrossRef]
2. Glatter, K.; Finkelman, P. History of the Plague. History of the Plague: An Ancient Pandemic for the Age of COVID-19. *Am. J. Med.* **2021**, *134*, 177–180. [CrossRef] [PubMed]
3. Fonseca Azevedo Araújo, K.M.; Medeiros Leano, H.A.; Nogueira Rodrigues, R.; Caux Bueno, I.; Félix Lana, F.C. Epidemiological trends of leprosy in an endemic state. *Rev. Rene* **2018**, *18*, 771–778. [CrossRef]
4. Qing, Z.; Liu, H.; Zhang, F. Prevention and Treatment of Leprosy. *China CDC Wkly.* **2019**, *2*, 53–56. [CrossRef]
5. Kermack, W.O.; McKendrick, A.G. A Contribution to the Mathematical Theory of Epidemics. laboratory of the Royal College of Physicians. *Proc. R. Soc. Lond. A* **1927**, *115*, 700–721. Available online: <https://royalsocietypublishing.org/> (accessed on 9 September 2022).
6. Capasso, V.; Serio, G. A generalization of the Kermack-Mckendrick deterministic epidemic model. *Math. Biosci.* **1978**, *42*, 43–61. [CrossRef]
7. Hurd, S.H.; Kaneene, J.B. The application of simulation models and systems analysis in epidemiology. *Prev. Vet. Med.* **1993**, *15*, 81–99. [CrossRef]
8. Keeling, M.J. Networks and Epidemic Models. *J. R. Soc. Interface* **2005**, *2*, 295–307. [CrossRef]
9. Newman, M. *Networks: An Introduction*; Oxford University Press: Oxford, UK, 2010.
10. Fauci, A.S. Emerging and Reemerging Infectious Diseases: The Perpetual Challenge. *Acad. Med.* **2005**, *80*, 1079–1085. [CrossRef]

11. Fiore, V.G.; DeFelice, N.; Glicksberg, B.S.; Perl, O.; Shuster, A.; Kulkarni, K.; O'Brien, M.; PISAURO, M.A.; Chung, D.; Gu, X. Containment of COVID-19: Simulating the impact of different policies and testing capacities for contact tracing, testing, and isolation. *PLoS ONE* **2021**, *16*, e0247614. [[CrossRef](#)]
12. Hendrix, K.S.; Sturm, L.A.; Zimet, G.D.; Mesli, E.M. Ethics and Childhood Vaccination Policy in the United States. *Am. J. Public Health* **2016**, *106*, 273–278. [[CrossRef](#)]
13. Jefferson Ribeiro da Silva, S.; Cristina de Lima, S.; Celerino da Silva, R.; Kohl, A.; Pena, L. Viral Load in COVID-19 Patients: Implications for Prognosis and Vaccine Efficacy in the Context of Emerging SARS-CoV-2 Variants. *Front. Med.* **2022**, *8*, 836826. [[CrossRef](#)]
14. Loy, N.; Tosin, A. A viral load-based model for epidemic spread on spatial networks. *Math. Biosci. Eng.* **2021**, *18*, 5635–5663. [[CrossRef](#)]
15. Mafalda, M.N.S.; Pimentel, V.; Torneri, A.; Seabra, S.G.; Libin, P.J.K.; Abecasis, A.B. A Tale of Three Recent Pandemics: Influenza, HIV and SARS-CoV-2. *Front. Microbiol.* **2022**, *13*, 889643. [[CrossRef](#)]
16. Zuin, M.; Gentili, V.; Cervellati, C.; Rizzo, R.; Zuliani, G. Viral Load Difference between Symptomatic and Asymptomatic COVID-19 Patients: Systematic Review and Meta-Analysis. *Infect. Dis. Rep.* **2021**, *13*, 645–653. [[CrossRef](#)]
17. Puhach, O.; Meyer, B.; Eckerle, I. SARS-CoV-2 viral load and shedding kinetics. *Nat. Rev. Microbiol.* **2022**, *2022*. [[CrossRef](#)]
18. Hethcote, H.W. The Mathematics of Infectious Diseases. *Soc. Ind. Appl. Math.* **2000**, *42*, 599–653. [[CrossRef](#)]
19. Iranzo, V.; Pérez-González, S. Epidemiological models and COVID-19: A comparative view. *Hist. Philos. Life Sci.* **2021**, *43*, 104. [[CrossRef](#)]
20. Douskos, C.; Markellos, P. Complete Coefficient Criteria for Five-Dimensional Hopf Bifurcations, with an Application to Economic Dynamics. *J. Nonlinear Dyn.* **2015**, *2015*, 278234. [[CrossRef](#)]
21. Ottaviano, S.; Sensi, M.; Sottile, S. Global stability of SAIRS epidemic models. *Nonlinear Anal. Real World Appl.* **2022**, *65*, 103501. [[CrossRef](#)]
22. Lord, A.; Ernstberger, S. Modeling COVID-19 Data using an SIR Model. *Cit. J. Undergrad. Res.* **2021**, *18*, 133–136.
23. Violato, C.; Violato, E.M.; Violato, E.M. Impact of the stringency of lockdown measures on COVID-19: A theoretical model of a pandemic. *PLoS ONE* **2021**, *16*, e0258205. [[CrossRef](#)] [[PubMed](#)]
24. Ashcroft, P.; Lehtinen, S.; Angst, D.C.; Low, N.; Bonhoeffer, S. Quantifying the impact of quarantine duration on COVID-19 transmission. *Elife* **2021**, *10*, e63704. [[CrossRef](#)] [[PubMed](#)]
25. Teslya, A.; Rozhnova, G.; Pham, T.; Van Wees, D.; Nunner, H.; Godijk, N.; Bootsma, M.; Kretzschmar, M. The importance of sustained compliance with physical distancing during COVID-19 vaccination rollout. *Commun. Med.* **2022**, *2*, 146. [[CrossRef](#)] [[PubMed](#)]
26. Piccirillo, V. COVID-19 pandemic control using restrictions and vaccination. *Math. Biosci. Eng.* **2022**, *19*, 1355–1372. [[CrossRef](#)]
27. Kojakhmetov, H.J.; Kuehn, C.; Pugliese, A.; Sens, M. A geometric analysis of the SIRS epidemiological model on a homogeneous network. *J. Math. Biol.* **2021**, *83*, 37. [[CrossRef](#)]
28. Lobinska, G.; Pauzner, A.; Traulsen, A.; Pilpel, Y.; Nowak, M.A. Evolution of resistance to COVID-19 vaccination with dynamic social distancing. *Nat. Hum. Behav.* **2022**, *6*, 193–206. [[CrossRef](#)]
29. Buonomo, B.; d'Onofrio, A.; Lacitignolac, D. Global stability of an SIR epidemic model with information dependent vaccination. *Math. Biosci.* **2008**, *216*, 9–16. [[CrossRef](#)]
30. Rao, I.J.; Brandeau, M.L. Sequential allocation of vaccine to control an infectious disease. *Math. Biosci.* **2022**, *351*, 108879. [[CrossRef](#)]

**Disclaimer/Publisher's Note:** The statements, opinions and data contained in all publications are solely those of the individual author(s) and contributor(s) and not of MDPI and/or the editor(s). MDPI and/or the editor(s) disclaim responsibility for any injury to people or property resulting from any ideas, methods, instructions or products referred to in the content.